Tryptophan Scanning of D1S6 and D4S6 C-Termini in Voltage-Gated Sodium Channels

Sho-Ya Wang,* Kaitlin Bonner,* Corinna Russell,† and Ging Kuo Wang†
*Department of Biology, State University of New York at Albany, Albany, New York; and †Department of Anesthesia, Harvard Medical School and Brigham and Women's Hospital, Boston, Massachusetts

ABSTRACT Recent reports suggest that four S6 C-termini may jointly close the voltage-gated cation channel at the cytoplasmic side, probably as an inverted teepee structure. In this study we substituted individually a total of 18 residues at D1S6 and D4S6 C-terminal ends of the rNav1.4 Na^+ channel α-subunit with tryptophan (W) and examined their corresponding gating properties when expressed in Hek293t cells along with β1 subunit. Several W-mutants displayed significant changes in activation, fast inactivation, and/or slow inactivation gating. In particular, five S6 W-mutants showed incomplete fast inactivation with noninactivating maintained currents present. Cysteine (C) substitutions of these five residues resulted in two mutants with slightly more maintained currents. Multiple substitutions at these five positions yielded two mutants (L437C/A438W, L435W/L437C/A438W) that exhibited phenotypes with minimal fast inactivation. Unexpectedly, such inactivation-deficient mutants expressed Na^+ currents as well as did the wild-type. Furthermore, all mutants with impaired fast inactivation exhibited an enhanced slow inactivation phenotype. Implications of these results will be discussed in terms of indirect allosteric modulations via amino acid substitutions and/or a direct involvement of S6 C-termini in Na^+ channel gating.

INTRODUCTION

Voltage-gated Na^+ channels are pore-forming membrane proteins responsible for the generation of action potentials in excitable membranes. These ion channels consist of one large α-subunit and one or two smaller β-subunits (β1, β2, and β3) (Catterall, 2000). The Na^+ channel α-subunit isoforms contain four homologous repeated domains (D1–D4), each with six transmembrane segments (S1–S6). The α-subunit protein alone forms a functional channel when expressed in mammalian expression systems (Ukomadu et al., 1992). The four repeated domains probably assemble as a peudotetrameric structure with the permeation pathway situated at the center.

Several pieces of evidence suggest that S6 segments are important for Na^+ channel gating. First, a number of receptors for various therapeutic drugs and neurotoxins such as local anesthetics, antiarrhythmics, anticonvulsants, antidepressants, pyrethroid insecticides, batrachotoxin (BTX), and veratridine are situated at the middle of multiple S6 segments (Fig. 1) (Wang and Wang, 2003). Upon binding, these ligands exert their pharmacological actions on the Na^+ channel, presumably in part via their corresponding S6 receptor. In particular, BTX modifies Na^+ channel activation, fast inactivation, and slow inactivation drastically, suggesting that its receptor is linked to these gating processes. Second, S6 segments may be structurally geared for channel activation since alanine substitutions at their C-termini cause significant changes in Na^+ channel activation (Yarov-Yarovoy et al., 2002). Consistent with this view, activation of voltage-gated K^+ channels also requires lateral/rotational movements of S6 segments at their constricted C-termini. One possible mechanism for the lateral/rotational movement is via a flexible gating hinge, a glycine residue located at the middle of the inner transmembrane segments of KcsA channels (M2) (Jiang et al., 2002). Such a glycine residue is also present in Na^+ channel S6 segments of D1, D2, and D3 (Fig. 1, *dashed box*). This gating hinge could have two different conformations. One is in its relaxed straight α-helical form, which closes the channel at the S6 C-terminal end, and the other is the bendable α-helical form, which may bend outward at a 30° angle and thus splay open the channel at the S6 constricted C-terminus. Third, after channel activation, S6 segments may then form the docking site for the fast-inactivation gate. A putative Na^+ channel inactivation gate has been delineated at the intracellular linker between D3 and D4 (West et al., 1992). This linker region contains an IFM motif, which is shown critical for the fast inactivation. The precise location of the docking site for this inactivation gate is unknown, but it could be situated at the C-termini of S6 segments (McPhee et al., 1995; Yarov-Yarovoy et al., 2002), where the inactivation gate may plug the open channel while binding to its docking site. This plugging mechanism has recently been demonstrated in voltage-gated K^+ channels (Zhou et al., 2001). Finally, several residues at S6 segments have been shown critical for the slow inactivation of Na^+ channels. One such substitution (V→M at position 23 in D1S6) enhances the slow inactivation (Takahashi and Cannon, 1999); this mutation also causes painful myotonic stiffness in humans (Rosenfeld, et al., 1997). The exact mechanism of the S6 involvement in slow inactivation gating remains unclear (Vilin and Ruben, 2001).

In this study we aimed to explore the functional role of the S6 C-terminal end with the tryptophan-scanning approach. The reason for this approach is relied on the concept that

Submitted January 16, 2003, and accepted for publication April 2, 2003.
Address reprint requests to Dr. Ging Kuo Wang, Dept. of Anesthesia, Brigham and Women's Hospital, 75 Francis St., Boston, MA 02115. Tel.: 617-732-6886; Fax: 617-730-2801; E-mail: wang@zeus.bwh.harvard.edu.

0006-3495/03/08/911/10 $2.00

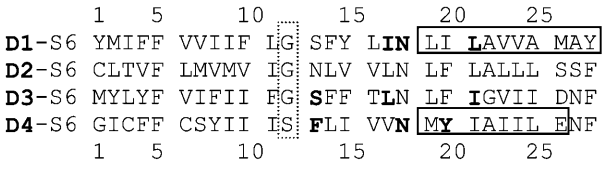

FIGURE 1 Sequences of S6 segments in D1–D4 of rNav1.4 Na^+ channel. Residues that influence binding of local anesthetics and/or BTX are in bold; most are clustered within ~3 helical turns. The dashed box at position 12 indicates the putative activation hinge, glycine/serine. The solid boxes indicate C-termini that were substituted with W.

substituted tryptophan (W), which contains a bulky hydrophobic side chain, may disrupt or alter channel function because of its large size. Such disruption or alteration may occur if tryptophan is substituted for an amino acid that contacts or directly interacts with other parts of the channel protein. Previously, using alanine-scanning mutagenesis, McPhee et al. (1995) and Yarov-Yarovoy et al. (2002) identified one residue (position 21) at D1S6 and two residues (position 13, 23) at D4S6 in Nav1.2 that are critical for fast inactivation. With W substitutions, we sought to confirm their alanine-scanning findings that the C-terminus of the S6 segment is important for gating functions. In addition, we sought to address whether the effects of several residues on the fast inactivation gating are additive after multiple tryptophan/cysteine substitutions and whether the slow inactivation and the fast inactivation have an apparent inverse relationship.

MATERIALS AND METHODS

Site-directed mutagenesis

We used the QuikChange XL Site-Directed Mutagenesis Kit (Stratagene, La Jolla, CA) to create rat skeletal muscle Nav1.4 mutant clones as described (Wang and Malcolm, 1999).

DNA sequencing near the mutated site confirmed these mutations. To minimize the possibility that unique phenotypes are due to unwanted mutations, we also created independent clones of rNav1.4-L435W/L437C/A438W and rNav1.4-L437C/A438W as well as additional homologous L435W/L437C/A438W clones from human isoforms (hNav1.4 and hNav1.5). Preliminary results showed that all of these independent and homologous clones displayed comparable phenotypes as those of rNav1.4 counterparts.

Transient transfection

Human embryonic kidney (Hek293t) cells were grown to ~50% confluence in Dulbecco's modified Eagle's medium (Life Technologies, Rockville, MD) containing 10% fetal bovine serum (HyClone, Logan, UT), 1% penicillin and streptomycin solution (Sigma, St. Louis, MO), 3 mM taurine, and 25 mM HEPES (Gibco) and then transfected by a calcium phosphate precipitation method in a Ti25 flask (Cannon and Strittmatter, 1993). Transfection of wild-type rNav1.4-pcDNA1/Amp or mutant clones (5–10 μg) along with β1-pcDNA1/Amp (10–20 μg) and reporter CD8-pih3m (1 μg) was adequate for later current recording. Cells were replated 15 h after transfection in 35-mm dishes, maintained at 37°C in a 5% CO_2 incubator, and used after 1–4 days. Transfection-positive cells were identified with immunobeads (CD8-Dynabeads, Lake Success, NY).

Whole-cell voltage clamp

Whole-cell configuration was used to record Na^+ currents (Hamill et al., 1981). Borosilicate micropipettes (Drummond Scientific Company, Broomall, PA) were pulled with a puller (P-87, Sutter Instrument Company, Novato, CA) and heat polished. Pipette electrodes contained 100 mM NaF, 30 mM NaCl, 10 mM EGTA, and 10 mM HEPES adjusted to pH 7.2 with CsOH. The pipette electrodes had a tip resistance of 0.5 to 1.0 MΩ. Access resistance was 1–2 MΩ and was further reduced by series resistance compensation. All experiments were performed at room temperature (22–24°C) under a Na^+-containing bath solution with 65 mM NaCl, 85 mM choline Cl, 2 mM $CaCl_2$, and 10 mM HEPES adjusted to pH 7.4 with tetramethyl-ammonium hydroxide. Residual outward currents were evident in some cells at voltages $\geq +30$ mV (Wang and Wang, 1998); these currents were present in untransfected cells and were insensitive to tetradotoxin. We might overestimate the maintained currents slightly since these residual currents were not subtracted from our measurements. Whole-cell currents were measured by an Axopatch 200B (Axon Instruments, Foster City, CA) or an EPC-7 (List Electronics, Darmstadt/Eberstadt, Germany), filtered at 3 kHz, collected, and analyzed with pClamp8 software (Axon Instruments). Leak and capacitance were subtracted by the patch clamp device and further by the leak subtraction protocol (P/−4). Cells were held at −140 mV for functional characterizations. Voltage error was <4 mV after series resistance compensation. An unpaired Student's *t*-test was used to evaluate estimated parameters (mean ± SE or fitted value ± SE of the fit); *p*-values of <0.05 were considered statistically significant.

RESULTS

Gating properties of W substitutions within the C-terminus of D1S6 in Nav1.4 Na^+ channels

We substituted individual D1S6 residues at the C-terminus (Fig. 1; *solid box*) with tryptophan. To characterize the effects of W substitutions, we measured Na^+ currents of D1S6 W-substituted mutant channels at various voltages. As an example, Fig. 2, *A* and *B* shows the superimposed current families of Nav1.4 wild-type and mutant Nav1.4-A438W (position 22 at D1S6) cotransfected with β1 subunit, respectively. Activation threshold was around −50 mV for wild-type and around −60 mV for A438W mutant channels. The peak conductance was calculated as described in the figure legend, normalized, and plotted against the corresponding voltage (Fig. 2 *C*). Voltage dependence of activation was fitted by a standard Boltzmann equation, and the W mutant showed an apparent leftward shift of −6.8 ± 2.1 mV ($n = 6$). Fig. 3 lists all W mutants at the C-terminus of the D1S6 region (Fig. 3; *top left*). Except for L435W and I436W, all other D1S6 mutants W displayed a leftward shift. L437W shifted leftward by as much as −22.1 ± 2.0 mV ($n = 5$). The slope factor for each W mutant was either no significant change or became less steep. One mutant, V439W, did not express sufficient Na^+ currents (<1 nA) in our experiments.

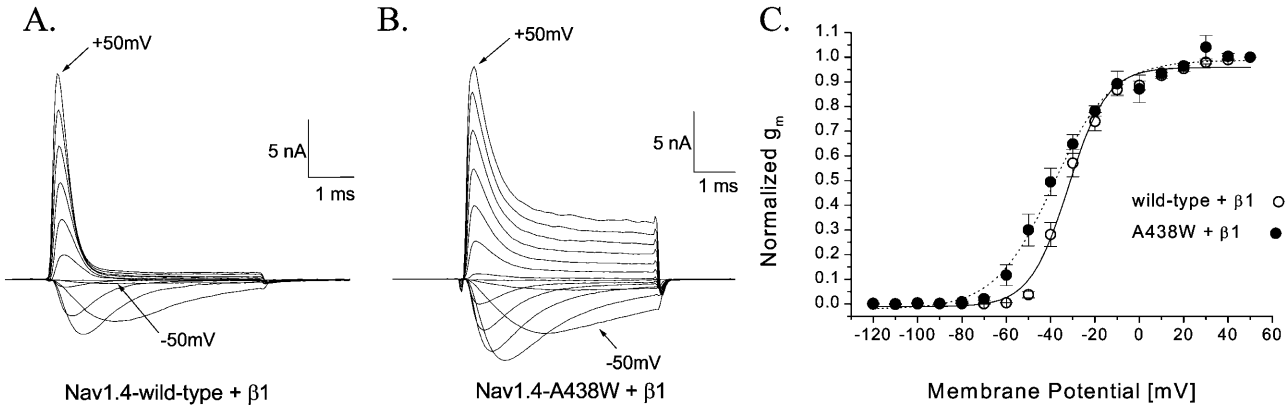

FIGURE 2 Activation of wild-type and rNav1.4-A438W coexpressed with β1. Families of Na^+ currents for wild-type (*A*) and Nav1.4-A438 mutant (*B*) were evoked by 5-ms pulses from the holding potential (−140 mV) to voltages ranging from −120 to +50 mV in 10-mV increments. The current traces evoked by a pulse to −50 mV and to +50 mV are labeled. Cells were cotransfected with β1 subunit. (*C*) Normalized membrane conductance (g_m) was determined from the equation $g_m = I_{Na}/(E_m - E_{Na})$, where I_{Na} is the peak current, E_m is the amplitude of the pulse voltage, and E_{Na} is the reversal potential, and plotted against the pulse voltage. Plots were fitted with a Boltzmann function, which yielded the midpoint voltage ($V_{0.5}$) and slope (k) for wild-type (*open circles*, $n = 5$) of −32.0 ± 0.9 mV and 8.7 ± 0.8 mV, respectively, and −38.8 ± 1.2 mV and 13.1 ±1.1 mV for rNav1.5-A438W (*closed circles*, $n = 6$).

Another noticeable change in gating after A438W substitution was the noninactivating currents maintained at the end of the pulse (Fig. 2 *B* versus Fig. 2 *A*). To quantify this difference between wild-type and mutant channels we measured the amount of the noninactivating maintained current near the end of 5-ms +50 mV pulse. The wild-type current decayed rapidly and reached its steady-state level within 2–3 ms and 2.9 ± 0.8% ($n = 5$) of currents were maintained under these experimental conditions (Fig. 2 *A* and Fig. 4). In contrast, Nav1.4-A438W mutant showed conspicuous maintained currents under identical conditions; 31.9 ± 4.2% ($n = 6$) of currents were noninactivating as measured near the 5-ms time. Thus, a substitution of W at position 22 of D1S6 impairs the Na^+ channel fast inactivation significantly ($p < 0.001$). This 22 position at D1S6 was not studied previously using an alanine-scanning approach because the native residue was an alanine amino acid. The relative noninactivating components of all mutants at D1S6 are listed in Fig. 4 (*left section*). The two other W mutants with impaired fast inactivation are L435W (Fig.4; the fraction of noninactivating current = 0.10 ± 0.02, $n = 5$, $p < 0.05$; position 18) and L437W (0.055 ± 0.017, $n = 5$, $p = 0.20$; position 21).

Using various conditioning pulses from −160 mV to −15 mV, we further characterized the steady-state inactivation of the mutant channels. Fig. 5, *A* and *B*, shows Na^+ currents of the wild-type and Nav1.4-A438W mutant, respectively, under these pulse conditions. Peak currents were measured, normalized with respect to the peak current at −160 mV, and plotted against conditioning voltages (Fig. 5 *C*). Clearly, a noninactivating component was again present in Nav1.4-A438W mutant channels. The data were fitted with a standard Boltzmann equation, and the shift in the $\Delta V_{0.5}$ is shown in Fig. 3 (*top right*) along with the shift in the slope factor, the Δk value.

Gating properties of tryptophan substitutions within the C-terminus of D4S6

We also substituted individual D4S6 residues from position 19 to 26 with tryptophan (Fig. 1; *solid box*). Fig. 6, *A* and *B* shows the current voltage relationship and steady-state inactivation measurement of mutant Nav1.4-I1589W, respectively. Fig. 6 *C* shows the normalized peak conductance and h_∞ measurements against voltage of this mutant channel. Again there were significant noninactivating currents maintained at the end of test pulse for I1589W. The relative amounts of the maintained currents of all mutants at D4S6 are listed in Fig. 4 (*middle section*) along with D1S6 mutants. The activation of I1589W was shifted rightward by 13.0 ± 1.9 mV ($n = 6$), and the steady-state inactivation was shifted rightward by 6.8 ± 0.3 mV ($n = 5$). These changes in gating parameters of all D4S6 mutants are listed in Fig. 3 (middle section). Two W mutant channels (I1589W and I1590W) appeared to have significantly impaired fast inactivation. Two mutants, I1587W and A1588W, did not express sufficient Na^+ currents (<1 nA) in this expression system.

Gating properties of cysteine substitutions at selected residues within D1S6 and D4S6

It is unclear why tryptophan substitutions caused several residues with impaired fast inactivation. If the bulky W residues interfered with lateral or rotational movement of S6 segments, a smaller residue such as cysteine should have lesser effects. We found that there was no clear relationship with the size of residues and the degree of the impairment in fast inactivation. Fig. 7, *A* and *B* shows the current families of A438C and I1589C, respectively. A438W and I1590W exhibited significantly impaired fast inactivation but A438C

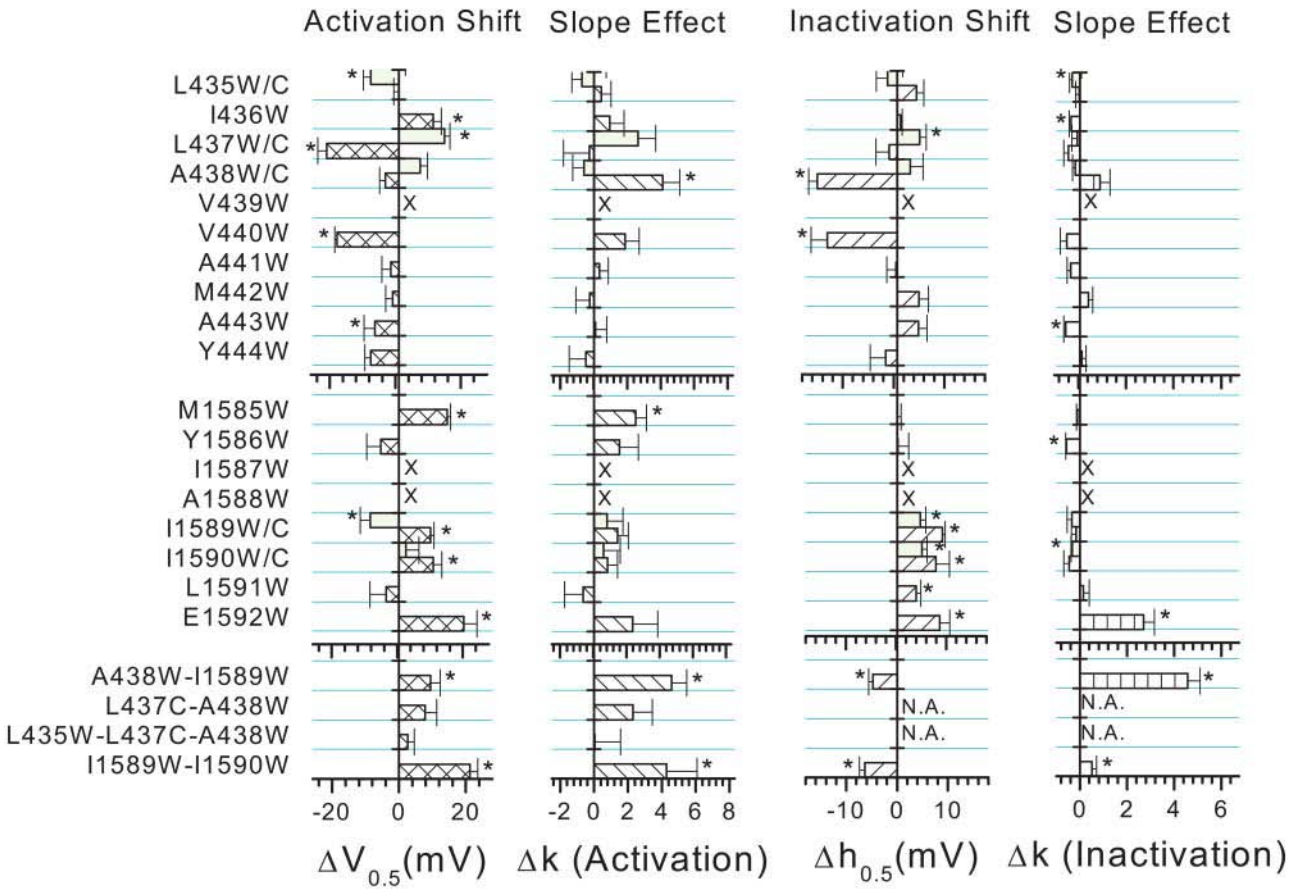

FIGURE 3 Summary of effects of W- and selected C-mutations at C-termini of D1S6 and D4S6 on activation and inactivation gating. *Left panel*: Vertical representation of amino acid sequence of D1S6 (*top*), D4S6 (*middle*), and double and triple mutants (*bottom*). All mutants and wild-type Na^+ channels were cotransfected with the $\beta 1$ subunit. *Activation shift:* the bar graph shows the differences in voltage for the half-maximal activation ($V_{0.5}$) of the wild-type and mutant Na^+ channels. The $V_{0.5}$ values (mean ± SE) were obtained from the Boltzmann fits of normalized conductance versus voltage plots as described in the legend of Fig. 2. The estimated reversal potential (E_{Na}) remained about the same in these mutants. Bars in gray indicate single C-substitution. Nonexpressing mutants are noted with an X. *Slope effect (activation, inactivation)*: the bar graph shows the differences in k values for the wild-type and mutant channels. The k values (mean ± SE) were obtained from Boltzmann fits of *I/V* plots (*activation*) and from Boltzmann fits of steady-state inactivation plots (*inactivation*), as described in the legend to Figs. 2 and 5, respectively. *Inactivation shift*: the bar graph shows the differences in voltage for the half-maximal inactivation ($h_{0.5}$) of the wild-type and mutant Na^+ channels. The $h_{0.5}$ values (mean ± SE) were obtained as described in the legend to Fig. 5. All values were derived from $n = 4$–6, except E1592W with $n = 3$. Asterisk indicates that the value is statistically different from that of the wild-type ($p < 0.05$).

and I1590C did not (Figs. 2 and 4). In contrast, I1589C displayed similar impaired fast inactivation as I1589W did (Fig. 4). This lack of direct correlation in volume suggests that the volume increase by bulky W substitution in some mutants is not the primary cause for their impaired fast inactivation. Instead, our results suggest that either allosteric effects occur after amino acid substitutions or these residues may interact with other parts of channel structure specifically and directly, such as the inactivation gate.

Yarov-Yarovoy et al. (2002) reported the only mutant within D1S6 that displayed maintained currents of about 10% control peak current was Nav1.2-L421C, which is equivalent to Nav1.4-L437C. Nav1.2-L421A did not express sufficient Na^+ currents in their study. We found that Nav1.4-L437C did display a slightly larger maintained current than the wild-type and L437W mutant but the difference was not statistically significant.

Gating properties of double and triple substitutions of selected residues within D1S6 and D4S6

We tested whether the effects of selected residues (L435, L437, A438, I1589, I1590) on the fast inactivation gating were additive with multiple substitutions. Several multiple-substituted mutants expressed a high level of Na^+ currents comparable to that of wild-type. We found two distinct types of phenotypes on these mutants. One type showed supra-additive effects on the fast inactivation, and the other showed subadditive effects. Fig. 8, *A–D* shows the current families of A438W/1589W, L437C/A438W, L435W/L437C/A438W,

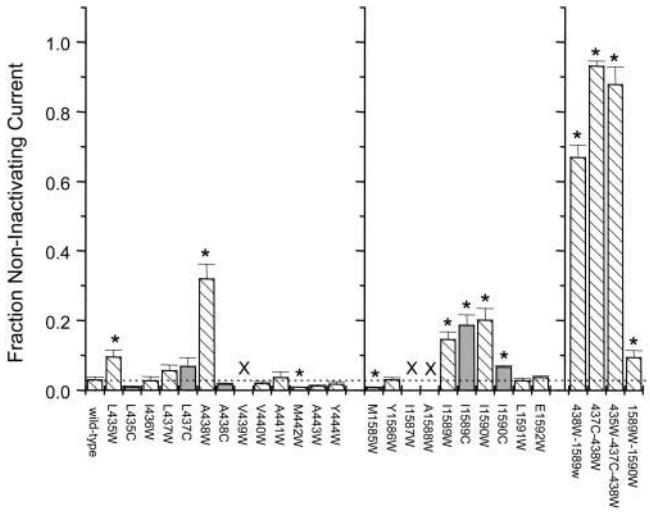

FIGURE 4 Relative maintained currents in various W- and C-mutations at C-termini of D1S6 and D4S6. Fraction of noninactivating current for D1S6 mutants (*left*), D4S6 (*middle*), and double and triple mutants (*right*). Cells were cotransfected with $\beta 1$ subunit; nonexpressing mutants are noted with an X. The fraction of noninactivating current was determined as the averaged current amplitude near 5 ms after the +50 mV pulse (e.g., Fig. 2) divided by the peak current. Error bars indicate standard error. Asterisks indicate significant differences from the wild-type channels as determined by a *t*-test ($p < 0.05$, $n = 4$–6). Dotted line indicates the value of wild-type. Bars in gray indicate single C-substitution.

and I1589W/I1590W, respectively. Clearly, I1589W/I1590W is the one that displayed equal or lesser effects on the fast inactivation than the single substitution (Fig. 8 *D* versus Fig. 6 *A*), whereas the others showed the opposite. The gating parameters of these mutants were listed in Fig. 3 (*bottom*) and Fig. 4 (*right*). One mutant (A438W/I1590W) expressed insufficient Na^+ currents for these measurements. Our results thus demonstrate that it is feasible to create fast-inactivation deficient mutants that express rather well in the mammalian expression system. These S6 mutants are distinct from the IFM→QQQ mutant, which expresses rather poorly in Hek293t cells but readily in *Xenopus* oocytes.

Inverse relationship between fast inactivation and slow inactivation gating?

When the fast inactivation is hampered by pronase or by site-directed mutagensis, slow inactivation gating not only remained functional but also was accelerated considerably. This inverse relationship suggested that the fast inactivation and slow inactivation gating have distinct identities, and yet these two gating processes are somehow coupled. To determine whether such inverse relationship holds true in S6 mutants with severely impaired fast inactivation, we therefore measured the slow inactivation gating with a 10-s conditioning prepulse at various voltages. With a gap of 100 ms at −140 mV, which allowed channels recovered from their fast inactivation but not from their slow inactivation, we observed that 57.1 ± 3.6% ($n = 5$) of wild-type Na^+ currents were slow inactivated at 0 mV for 10 s (Fig. 9 *A*; *open circles*). In contrast, almost all L435W/L437C/A438W mutant channels were slow-inactivated (Fig. 9 *A*, *closed circles*) at 0 mV under these experimental conditions. It appeared that this enhanced slow inactivation is in part due to the enhanced forward rate constant as shown in Fig. 9 *B*. Multiple-substituted mutants with enhanced slow inactivation were inactivated with a rather rapid rate, with a time constant of < 1 s at +30 mV (vs. 4.8 s for wild-type). It is noteworthy that slow inactivation in wild-type channels does not reach its steady state with a 10-s conditioning pulse even at +30 mV (Fig. 9 *B*). Nonetheless, this pulse protocol

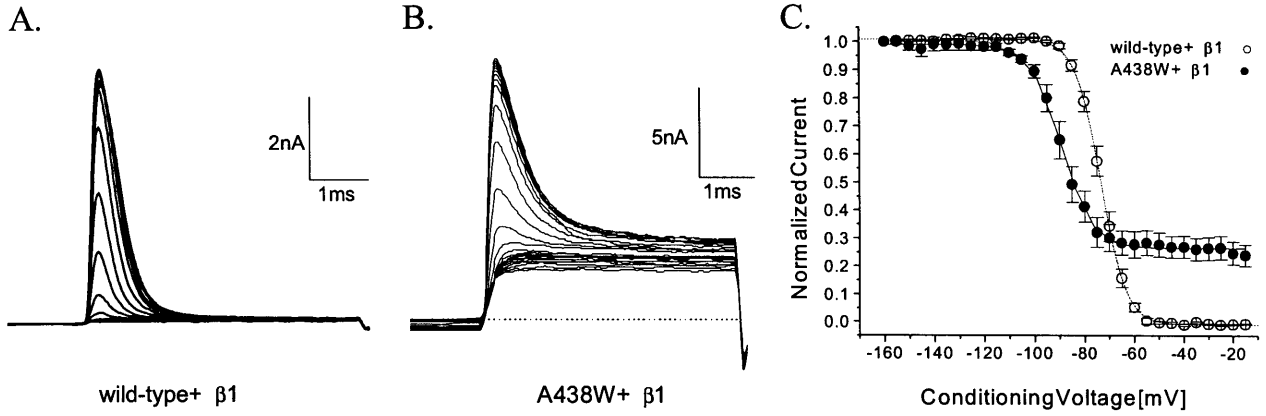

FIGURE 5 Steady-state inactivation of wild-type and rNav1.4-A438W coexpressed with $\beta 1$. Superimposed Na^+ currents of wild-type (*A*) and rNav1.4-A438W mutant (*B*) were evoked by a 5-ms test pulse to +30 mV. Test pulses were preceded by 100-ms conditioning pulses ranging from −160 mV and −15mV in 5-mV increments. Notice that small noninactivating inward currents appeared at conditioning voltages ≥ −60 mV. Cells were cotransfected with $\beta 1$ subunit. (*C*) Normalized Na^+ current availability (h_∞) of wild-type (*open circle*, $n = 5$) and rNav1.4-A438W (*closed circle*, $n = 5$) were plotted as a function of the 100-ms conditioning pulse voltage. Plots were fitted with the Boltzmann function. The fitted midpoint ($h_{0.5}$) and slope factor (k) for wild-type were −73.4 ± 0.1 mV and 5.0 ± 0.1 mV, respectively, and −89.0 ± 0.3 mV and 6.0 ± 0.2 mV for Nav1.4-A438W, respectively.

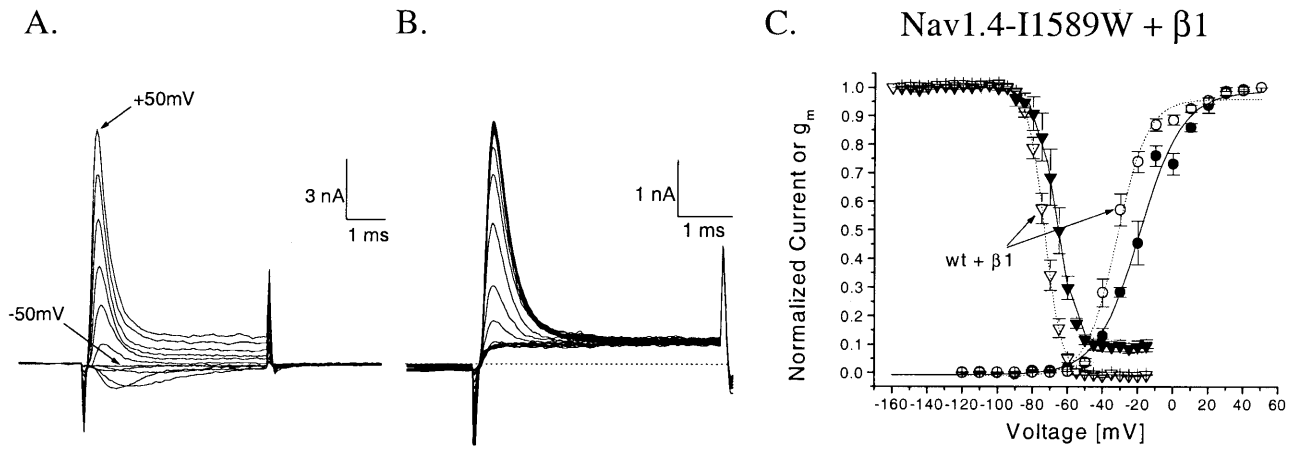

FIGURE 6 Gating properties of rNav1.4-I1589W coexpressed with β1. (*A*) Superimposed Na^+ current traces were evoked by 5-ms pulses from the holding potential (−140 mV) to voltages ranging from −120 to +50 mV in 10-mV increments. (*B*) Superimposed currents were evoked by a 5-ms test pulse to +30 mV preceded by 100-ms conditioning pulses ranging from −160 mV to −15mV in 5-mV increments. (*C*) Normalized Na^+ conductance (g_m) was derived from (*A*) as described in the Fig. 2 legend, plotted against voltage, and fitted with a Boltzmann function. The fitted midpoint voltage ($V_{0.5}$) and slope (k) of the function for wild-type (*open circles*, $n = 5$) were −32.0 ± 0.9 and 8.7 ± 0.8, respectively, and −19.0 ± 1.0 and 12.6 ± 0.9, respectively for rNav1.4-I1589W (*closed circles*, $n = 6$). Normalized Na^+ current availability (h_∞) of wild-type (*open down triangle*, $n = 5$) and Nav1.4-I1589W (*closed down triangle*, $n = 5$) were derived from (*B*) as described in the Fig. 5 legend, and plotted as a function of conditioning voltage. Plots were fitted with the Boltzmann function. The midpoint ($h_{0.5}$) and slope factor (k) for wild-type were −73.4 ± 0.1 and 5.0 ± 0.1, respectively, and −66.5 ± 0.2 and 5.7 ± 0.2, respectively, for the Nav1.4-I1589W. Cells were cotransfected with β1 subunit.

allowed us to determine which mutants exhibit altered slow inactivation significantly. Fig. 10 *A* lists the degree of slow inactivation, which varies in different mutants at −10 mV. I436 and E1592 are the only two mutants that appeared significantly less slow inactivated than the wild-type counterpart. In general, we observed that mutants with the most impaired fast inactivation (L435, L437, A438, I1589, I1590) were indeed also with enhanced slow inactivation. In particular, the multiple-substituted mutants, such as L437C/A438W and L435W/L437C/A438W, with the most impaired fast inactivation also had the most enhanced slow inactivation (Fig. 10 *B*). Our results therefore support that fast and slow inactivation processes have distinct entities, but these gating processes display an inverse relationship as if they are also somehow coupled in their structure. One interesting exception is the mutant I1589W/I1590W, which showed enhanced slow inactivation but with minimal impaired fast inactivation. This mutant is also unique since

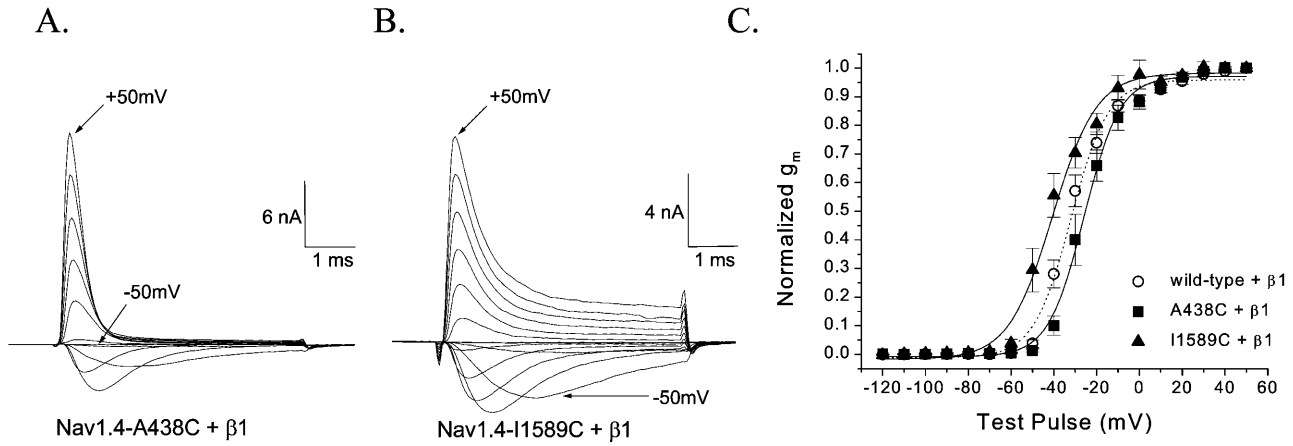

FIGURE 7 Activation of rNav1.4-A438C and rNav1.4-I1589C coexpressed with β1. Superimposed Na^+ current families of Nav1.4-A438C (*A*) and Nav1.4-I1589C (*B*) were evoked by 5-ms pulses from holding potential of −140 mV to voltages ranging from −120 to +50 mV in 10-mV increments. (*C*) Normalized membrane conductance (g_m) plotted versus the amplitude of the 5-ms voltage step. G_m was determined as described in the Fig. 2 legend, plotted against the membrane voltage, and fitted with a Boltzmann function. The fitted midpoint voltage ($V_{0.5}$) and slope (k) of the function for wild-type (*open circles*, $n = 5$) were −32.0 ± 0.9 and 8.7 ± 0.8, respectively, −25.9 ± 0.7 and 8.3 ± 0.6 for Nav1.4-A438C (*closed squares*, $n = 5$), and −39.9 ± 1.1 and 10.9 ± 0.9 for Nav1.4-I1589C (*closed triangles*, $n = 6$). Cells were cotransfected with β1 subunit.

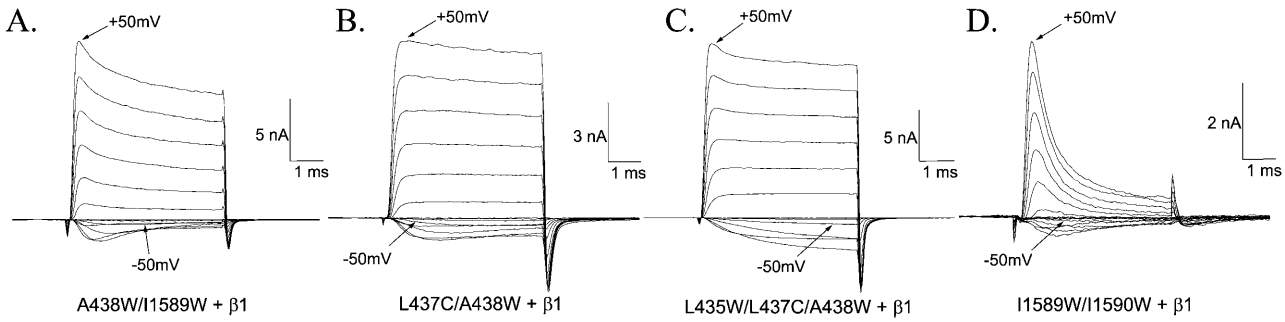

FIGURE 8 Activation gating of double and triple mutants. Superimposed Na^+ current families were evoked by 5-ms pulses from holding potential of −140 mV to voltages ranging from −120 to +50 mV in 10-mV increments for mutants A438W/I1589W (*A*), L437C/A438W (*B*), L435W/L437C/A438W (*C*), and I1589W/I1590W (*D*). All mutants were cotransfected with the $\beta 1$ subunit.

each single substitution in I1589W and I1590W shows impaired fast inactivation but far less in the double mutations (Fig. 4).

DISCUSSION

In this study we demonstrate that most mutants with a single W substitution at the C-terminus of D1S6 and D4S6 express sufficient Na^+ currents in Hek293t cells. Substitutions with W at this region may alter Na^+ channel activation, fast inactivation, and/or slow inactivation gating in variable degrees, dependent on the position of the substitution. In addition, we have identified five positions (L435, L437, A438, I1589, and I1590) critical for the fast inactivation gating. With multiple W or C substitutions, we have created two mutants (L437C/A438W and L435W/L437C/A438W) with minimal fast inactivation. Overall we obtain three major findings. First, five residues at positions 19, 21–22 at D1S6

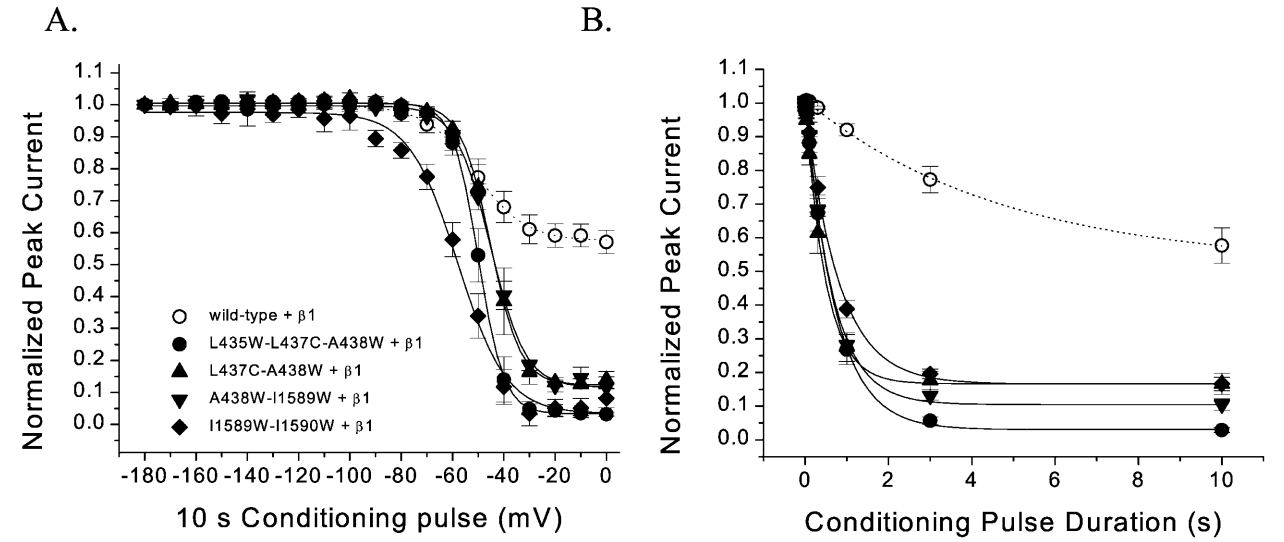

FIGURE 9 Slow inactivation gating of double and triple mutants. To induce slow inactivation, we applied conditioning prepulses ranging from −180 mV to 0 mV with a duration of 10 s. After a 100-ms interval at −140 mV, Na^+ currents were evoked by the delivery of a +30 mV test pulse. (*A*) Peak Na^+ currents were normalized to the corresponding current obtained with a prepulse to −180 mV and plotted against conditioning prepulse potential. Data were fitted with a Boltzmann function. The fitted $V_{0.5}$ values and k (slope factor) values from the Boltzmann functions were (in mV) −51.1 ± 0.5 and 9.7 ± 0.4, respectively, for wild-type (*open circles*, $n = 5$); −49.9 ± 0.1 and 5.0 ± 0.1, respectively, for L435W/L437C/A438W (*closed circles*, $n = 5$); −45.2 ± 0.3 and 5.8 ± 0.2, respectively, for L437C/A438W (*closed up triangles*, $n = 5$); −45.2 ± 0.3 and 6. 8 ± 0.3, respectively, for A438W/I1589W (*closed down triangles*, $n = 6$); and −50.0 ± 0.9 and 9.5 ± 0.8, respectively, for I1589W/I1590W (*closed diamonds*, $n = 5$). The final steady-state noninactivated values (in %) were 57.5 ± 0.4 (wild-type), 3.3 ± 0.4 (L435W/L437C/A438W), 12.3 ± 0.6 (L437C/A438W), 11.6 ± 0.8 (A438W/I1589W), and 3.4 ± 1.7 (I1589W/I1590W). All mutants are cotransfected with the $\beta 1$ subunit. (*B*) Development of slow inactivation. For the development of slow inactivation, the prepulse duration at +30 mV was varied ranging from 0 to 10s. The peak current at the test pulse of +30 was measured and normalized to the initial peak amplitude without a prepulse, and then plotted against the prepulse duration. The data were fitted by a single-exponential function. The τ values (and final steady-state Y_0 values) for wild-type, L435W/L437C/A438W, L437C/A438W, A438W/I1589W, and I1589W/I1590W are 4.8 ± 0.3 s (51.6%), 0.72 ± 0.01 s (3.0%), 0.50 ± 0.01 s (16.6%), 0.64 ± 0.02 s (10.5%), and 0.81 ± 0.02 s (16.6%), respectively.

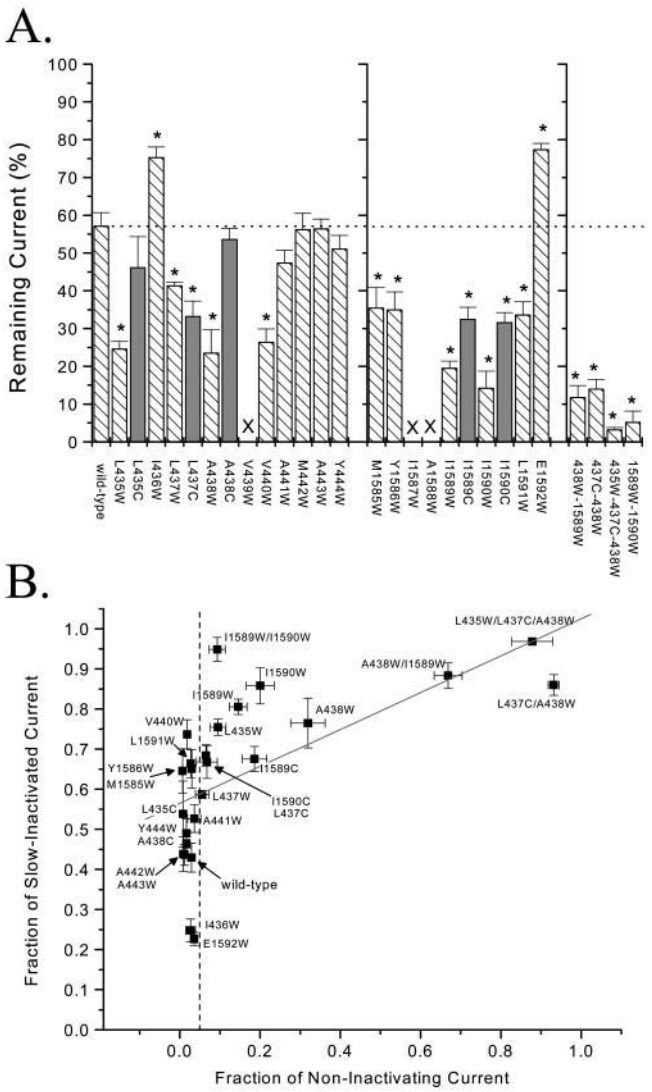

FIGURE 10 A coarse correlation between fast and slow inactivation gating. (*A*) The relative level of slow inactivation for D1S6 mutants (*left*), D4S6 (*middle*), and double and triple mutants (*right*). Nonexpressing mutants are noted with an X. Values represent mean ± SE of peak current elicited by a 5-ms test pulse to +30 mV preceded by a 10-s conditioning pulse to 0 mV and a 100-ms interval at −140 mV as described in Fig. 9 *A*. Asterisks indicate significant differences from the wild-type channels as determined by a *t*-test ($p < 0.05$). Dotted line indicates the value of wild-type. Bars in gray indicate single C-substitution. (*B*) The fraction of slow-inactivated current versus the fraction of noninactivating current of the individual mutant. Data for wild-type and mutants were taken from Fig. 4 for the *x* axis and from Fig. 10 *A* for the *y* axis. The mutants are labeled. The solid line is the linear fit of the complete data set with a correlation coefficient (*r*) of 0.61. Mutants with impaired fast inactivation (fraction of noninactivating current >5%) are shown at the right-hand side of the dashed line; all of them show enhanced slow inactivation.

and positions 23–24 at D4S6 are critical for the fast inactivation gating in Nav1.4 Na^+ channels. Two of the D1S6 residues have not been implicated before. Second, inactivation-deficient mutants with multiple substitutions express surprisingly well in Hek293t cells, unlike other mutants derived from the inactivation gate with the IFM motif at the D3–D4 cytoplasmic linker. Third, all mutants with impaired fast inactivation display an enhanced slow inactivation phenotype. We now discuss the significance of these results.

Mutations at C-terminal ends of D1S6 and D4S6 segments could affect Na^+ channel gating

Periodic changes in activation gating were reported in S6 segments using an alanine-scanning approach along with the *Xenopus* oocyte expression system (Yarov-Yarovoy et al., 2001, 2002). Mutations in the N-terminus and the middle part of the S6 segments caused small or little effects on the activation gating whereas mutations in the C-terminus had stronger effects on the voltage dependence of activation gating. With the W-scanning approach in the S6 C-terminal end we found that a few mutants indeed showed significant changes in their voltage dependence of activation gating. For example, mutants at D1S6 such as L437W, V440W, and A443W showed a negative shift of −22.1, −17.9, and −11.1 mV, respectively, whereas mutants at D4S6 such as E1592W, M1585W, I1589W, and I1590W had a positive shift of 18.6, 15.6, 13.0, and 10.2 mV, respectively. Thus, W-substitutions at D1S6 favor channel opening but do the opposite at D4S6 despite that slope factors for all these mutants became less steep (Fig. 3). These opposite effects of W-substitutions may be somehow due to the G/S conversion at the gating hinge, position 12 of D1S6 and D4S6 (Fig. 1). Yarov-Yarovoy, et al. (2002) suggested that the G/S conversion at D4S6 renders this segment less mobile. We also found that a smaller residue, cysteine, often displayed a small and opposite shift in activation gating. The shifts for W/C mutants at position L437, A438, I1589, and I1590 were −22.1/+13.5 mV, −6.8/+6.1 mV, +12.9/−7.9 mV, and +10.2/+2.6 mV, respectively. Therefore, at least for these four positions, activation properties are both position- and residue-specific. Our results nonetheless indicate that several residues at the C-terminus of D1S6 and D4S6 are critical for channel opening, in agreement with the alanine-scanning results (Yarov-Yarovoy et al., 2002).

McPhee et al (1994, 1995) and Yarov-Yarovoy (2001, 2002) reported the important roles of several residues at D1S6 and D4S6 on the fast inactivation gating process in brain Nav1.2 channels. One critical residue (Nav1.2-A422, which is Nav1.4-A438 equivalent) was not studied in their reports because it contains an alanine. Interestingly, the A438C mutant, unlike A438W, fails to affect the fast inactivation. Another W mutant with maintained current that was not identified by the alanine substitution in D1S6 is L435 (equivalent Nav1.2-L419A; Yarov-Yarovoy et al., 2002). The order of the level of the maintained current in D1S6/D4S6 residues is as follows: A438W (31.9%) > I1590W (20.0%) > I1589C (18.6%) > I1589W (14.5%) > L435W (9.5%) > L437C (6.7%) > L437W (5.5%) > wild-

type (2.9%). In contrast, only two mutants, M442W (0.9%) and M1585W (0.7%), displayed significantly less maintained currents than that of the wild-type. The amount of maintained current of L437W and L437C is higher than that of the wild-type, but it did not reach the level of statistic significance. In comparison, Nav1.2-L421C (equivalent to Nav1.4-L437C) has a maintained current of ~10% of the peak current, significantly higher than its wild-type (2%). Evidently, differences in the amount of maintained currents exist between mutants derived from different isoforms.

Probable cause for fast-inactivation deficiency in S6 mutants

We identify two clusters of adjacent residues, L437/A438 (position 21–22) and I1589/I1590 (position 23–24), which affect the fast inactivation severely. However, the L437/A438 effects on fast inactivation are supraadditive, whereas the I1589/I1590 effects are subadditive. In fact, the L437C showed only marginal effect on fast inactivation but when combined with A438W, it became an inactivation-deficient mutant (Figs. 4 and 8). One possible explanation is that substitutions at these positions cause allosteric changes in channel structures distant from these S6 C-terminal residues. The second possibility is that L437/A438 each interacts with a different amino acid or a different channel part so that the effect of each residue is supraadditive. This is possible because the adjacent residues are close enough within the α-helical structure, but their side chains are separated by ~110° in space. According to this reasoning, A438 and I1589 also interact with two separate amino acids since A438/I1589 effects are supraadditive. This interpretation is consistent with that of McPhee et al (1994, 1995) and Yarov-Yarovoy et al (2001, 2002), who suggested that the S6 C-termini may form the docking site for the fast inactivation gate. Alternatively, structural changes in S6 C-termini occur more extensively by the double mutations in L437C/A438W and A438W/I1589W than those by the single mutation. Unfortunately, mutant A438W/I1590W did not express and therefore yielded no useful information.

Inverse relationship between fast inactivation and slow inactivation

The magnitude of the slow inactivation and the fast inactivation appears to have an apparent inverse relationship. We found that the fraction of slow-inactivated channels followed the order I1590W (85.9%) > I1589W (80.6%) > A438W (76.6%) > L435W (75.5%) > L437W (58.7%) > wild-type (43.0%) as shown in Fig. 10 *B* at 0 mV; these mutants happened to be five residues with impaired fast inactivation. Furthermore, L435W/L437C/A438W, L437C/A438W, and A438W/I1589W mutants with multiple substitutions have minimal fast inactivation and they show significantly enhanced slow inactivation (96.8%, 93.2%, and 88.3%, respectively; Fig. 10 *B*). This inverse relationship is also common to other fast inactivation-deficient mutants, such as IFM→QQQ rNav1.4 mutant (e.g., Hilber et al., 2002), and inactivation-deficient Na^+ channels in pronase-treated squid axons (Rudy, 1978) or in chloramine-T treated rNav1.4 Na^+ channels (Wang and Wang, 1997).

One interpretation for this inverse relationship is that the S6 C-termini become wider during slow inactivation without the fast inactivation gate situated at its S6 docking site. This notion was recently proposed by Hilber et al. (2002). According to their model, the outward movement of S6 segments during slow inactivation causes the external P-loops to pinch inward which may constrict the permeation pathway (Ong et al., 2000; Vilin and Ruben, 2001). However, this external constriction site does not appear narrow enough to stop ion flow in voltage-gated Na^+ channels as the accessibility of residues located almost as deep as the selectivity filter remains the same for the external charged cysteine-modified reagent (Struyk and Cannon, 2002). Consequently, the slow inactivation gate in this model must be located right at the selectivity filter or its vicinity as suggested for the K^+ channel (Yellen, 1998).

Another interpretation for this inverse relationship is a narrowing of the C-termini of S6 segments during slow inactivation when the fast inactivation gate is no longer present at its docking site. This model is consistent with the facts that BTX binds preferentially to open Na^+ channels probably via the cytoplasmic side of permeation pathway (Li et al., 2002) but poorly to slow-inactivated Na^+ channels in normal as well as in pronase-treated squid axons by ~500-fold (Tanguy and Yeh, 1991). Such state-dependent binding of BTX could be due to the narrowing of S6 C-termini in inactivation-deficient Na^+ channels since the BTX binding site is likely adjacent to S6 C-termini (Wang and Wang, 2003). In contrast, widening of the S6 C-terminal region (Hilber et al., 2002) in the absence of the fast inactivation gate should, in theory, allow an easy access of BTX to its receptor (Li et al., 2002). This alternative model, however, does not imply that the S6 C-terminal region is sufficiently narrow to stop the ion flow during slow inactivation, as the size of BTX is far larger than that of the Na^+ ion. In any case, slow inactivation gating may require conformational changes that occur far apart both at the P-loop and S6 C-termini. Further studies are needed to delimit the location of the constricted site during slow inactivation.

High-level expression of mutants with minimal fast inactivation in Hek293t cells

We were surprised to find that the mutants with minimal fast inactivation express as well as the wild-type in Hek293t cells. Previous reports and our own attempts indicated that, unlike wild-type Na^+ channels, various fast-inactivation deficient mutants at the IFM motif expressed poorly in the Hek293t expression system under the same conditions. Grant

et al. (2000) suggested that the poor expression of IFM→QQQ mutant is due to loading of Na^+ ions in Hek293t cells because of the continuing opening of these mutant Na^+ channels. Several other factors could also affect the expression of inactivation-deficient mutants. For example, differences in activation and slow inactivation gating properties of these mutant channels; differences in post-translational modifications; and differences in protein folding, protein assembly, and subunit-subunit interactions may also influence the level of the channel expression. It is possible that S6 inactivation-deficient mutants express well in Hek293t cells with $\beta 1$ subunit because no spontaneous opening of these mutants occurs at the resting membrane potential of these cells. This could be due to a rightward shift in activation gating; +9.4, +7.5, and +5.2 mV for A438W/1589W, L437C/A438W, L435W/L437C/A438W, respectively. This could be also in part due to the significantly enhanced slow inactivation at the resting membrane potential. Further biochemical and biophysical comparisons of S6 inactivation-deficient mutants and IFM mutants may provide a direct answer to this question. In any event, these new inactivation-deficient S6 mutants will be useful tools for future studies, including the establishment of permanent cell lines, the screening for potent open-channel blockers that block persistent opening, the ion permeation in the persistent open channel, and the detailed studies on direct interactions between drugs and the open channel.

This work was supported by National Institutes of Health (HL66076).

REFERENCES

Cannon, S. C., and S. M. Strittmatter. 1993. Functional expression of sodium channel mutations identified in families with periodic paralysis. *Neuron.* 10:317–326.

Catterall, W. A. 2000. From ionic currents to molecular mechanisms: the structure and function of voltage-gated sodium channels. *Neuron.* 26: 13–25.

Grant, A. O., R. Chandra, C. Keller, M. Carboni, and C. F. Starmer. 2000. Block of wild-type and inactivation-deficient cardiac sodium channels IFM/QQQ stably expressed in mammalian cells. *Biophys. J.* 79:3019–3035.

Hamill, O. P., E. Marty, M. E. Neher, B. Sakmann, and F. J. Sigworth. 1981. Improved patch-clamp techniques for high-resolution current recording from cells and cell-free membrane patches. *Pflugers Arch.* 391:85–100.

Hilber, K., W. Sandtner, O. Kudlacek, B. Schreiner, I. Glasser, W. Schutz, H. A. Fozzard, S. C. Dudley, and H. Todt. 2002. Interaction between fast and ultra-slow inactivation in the voltage-gated sodium channel. *J. Biol. Chem.* 277:37105–37115.

Jiang, Y., A. Lee, J. Chen, M. Cadene, B. T. Chait, and R. MacKinnon. 2002. The open pore conformation of potassium channels. *Nature.* 417:523–526.

Li, H.-L., D. Hadid, and D. S. Ragsdale. 2002. The batrachotoxin receptor on the voltage-gated sodium channel is guarded by the channel activation gate. *Mol. Pharmacol.* 61:905–912.

McPhee, J. C., D. S. Ragsdale, T. Scheuer, and W. A. Catterall. 1995. A critical role for transmembrane segment IVS6 of the sodium channel alpha subunit in fast inactivation. *J. Biol. Chem.* 270:12025–12034.

McPhee, J. C., D. S. Ragsdale, T. Scheuer, and W. A. Catterall. 1994. A mutation in segment IVS6 disrupts fast inactivation of sodium channels. *Proc. Natl. Acad. Sci. USA.* 91:12346–12350.

Ong, B.-H., G. F. Tomaselli, and J. R. Balser. 2000. A structural rearrangement in the sodium channel pore linked to slow inactivation and use dependence. *J. Gen. Physiol.* 116:653–661.

Rosenfeld, J., K. Sloan-Brown, and A. L. George. 1997. A novel muscle sodium channel mutation causes painful congenital myotonia. *Ann. Neurol.* 42:811–814.

Rudy, B. 1978. Slow inactivation of the sodium conductance in squid giant axons. Pronase resistance. *J. Physiol.* 283:1–21.

Struyk, A. F., and S. C. Cannon. 2002. Slow inactivation does not block the aqueous accessibility to the outer pore of voltage-gated Na channels. *J. Gen. Physiol.* 120:509–516.

Takahashi, M. P., and S. C. Cannon. 1999. Enhanced slow inactivation by V445M: a sodium channel mutation associated with myotonia. *Biophys. J.* 76:861–868.

Tanguy, J., and J. Z. Yeh. 1991. BTX modification of Na channels in squid axons. I. State dependence of BTX action. *J. Gen. Physiol.* 97:499–519.

Ukomadu, C., J. Zhou, F. J. Sigworth, and W. S. Agnew. 1992. μl Na^+ channels expressed transiently in human embryonic kidney cells: biochemical and biopysical properties. *Neuron.* 8:663–676.

Vilin, Y. Y., and P. Ruben. 2001. Slow inactivation in voltage-gated sodium channels. *Cell Biochem. Biophys.* 35:171–190.

Wang, S.-Y., and G. K. Wang. 1997. A mutation in segment I-S6 alters slow inactivation of sodium channels. *Biophys. J.* 72:1633–1640.

Wang, S.-Y., and G. K. Wang. 1998. Point mutations in segment I-S6 render voltage-gated Na^+ channels resistant to batrachotoxin. *Proc. Natl. Acad. Sci. USA.* 95:2653–2658.

Wang, S.-Y., and G. K. Wang. 2003. Voltage-gated sodium channels as primary targets of diverse lipid-soluble neurotoxins. *Cell. Signal.* 15: 151–159.

Wang, W., and B. A. Malcolm. 1999. Two-stage PCR protocol allowing introduction of multiple mutations, deletions and insertions using QuikChange Site-Directed Mutagenesis. *Biotechniques.* 26:680–682.

West, J. W., D. E. Patton, T. Scheuer, Y. Wang, A. L. Goldin, and W. A. Catterall. 1992. A cluster of hydrophobic amino acid residues required for fast Na^+ channel inactivation. *Proc. Natl. Acad. Sci. USA.* 89:10910–10914.

Yarov-Yarovoy, V., J. Brown, E. Sharp, J. J. Clare, T. Scheuer, and W. A. Catterall. 2001. Molecular determinants of voltage-dependent gating and binding of pore-blocking drugs in transmembrane segment IIIS6 of the Na^+ channel α subunit. *J. Biol. Chem.* 276:20–27.

Yarov-Yarovoy, V., J. C. McPhee, D. Idsvoog, C. Pate, T. Scheuer, and W. A. Catterall. 2002. Role of amino acid residues in transmembrane segments IS6 and IIS6 of the Na^+ channel α subunit in voltage-dependent gating and drug block. *J. Biol. Chem.* 277:35393–35401.

Yellen, G. 1998. The moving parts of voltage-gated ion channels. *Q. Rev. Biophys.* 31:239–295.

Zhou, M., J. H. Morais-Cabral, and R. MacKinnon. 2001. Potassium channel receptor site for the inactivation gate and quaternary amine inhibitors. *Nature.* 411:657–661.